MDPI

Article

Second harmonic generation from phase-engineered metasurfaces of nanoprisms

Kannta Mochizuki[1], Mako Sugiura[1], Hirofumi Yogo[1], Stefan Lundgaard[2], Jingwen Hu[2], Soon Hock Ng[2], Yoshiaki Nishijima[3,4], Saulius Juodkazis[2,4,5], Atsushi Sugita[1,*]

[1] Department of Applied Chemistry and Biochemical Engineering, Shizuoka University, 3-5-1 Johoku, Hamamatsu, Shizuoka 432-8561, Japan
[2] Optical Sciences Centre and ARC Training Centre in Surface Engineering for Advanced Materials (SEAM), School of Science, Swinburne University of Technology, Hawthorn, VIC 3122, Australia
[3] Department of Physics, Electrical and Computer Engineering, Graduate School of Engineering, Yokohama National University, 79-5 Tokiwadai, Hodogaya-ku, Yokohama 240-8501, Japan
[4] Institute of Advanced Sciences, Yokohama National University, 79-5 Tokiwadai, Hodogaya-ku, Yokohama 240-8501, Japan
[5] World Research Hub Initiative (WRHI), School of Materials and Chemical Technology, Tokyo Institute of Technology, 2-12-1, Ookayama, Meguro-ku, Tokyo 152-8550, Japan
* Correspondence: A.S. sugita.atsushi@shizuoka.ac.jp

Version August 10, 2020 submitted to Micromachines

Abstract: Metasurfaces of gold (Au) nanoparticles on a SiO_2-Si substrate were fabricated for the enhancement of second harmonic generation (SHG) using electron beam lithography and lift-off. Triangular Au nanoprisms which are non-centro-symmetric and support the second- order non-linearity were examined for SHG. The thickness of the SiO_2 spacer is shown to be an efficient parameter to spectrally tune to maximise SHG. Electrical field enhancement at the fundamental wavelength was shown to define the intensity of the second harmonics. Numerical modeling of light enhancement was verified by experimental measurements of SHG and reflectivity spectra at the normal incidence. At the plasmonic resonance, SHG is enhanced up to $\sim 3.5 \times 10^3$ times for the optimised conditions.

Keywords: metasurfaces, second harmonic generation, phase control, finite difference time domain

1. Introduction

Energy up-conversion is important for very different fields: non-linear optics (NLO) and generation of higher laser harmonics, harvesting of long-wavelength, sub-bandgap energy light in solar cells, and photo-thermal excitation of neurons at the near-IR transparency window in tissue [1–3]. Creating efficient strategies for generation of second and higher harmonics of light using non-linear $\chi^{(2)}$ and $\chi^{(3)}$ response of metasurfaces is a recent and active line of research [4–8]. At the nanoscale, phase matching conditions that are required for efficient energy transfer from the fundamental wavelength λ into higher harmonic $\lambda/2$ along the co-propagation direction is relaxed at the near-field, however, the efficiency of the second harmonic generation (SHG) is low. It can only be compensated by the field enhancement and geometrical factors of the nanoparticles. For example, an array of gold nano-bumps made by controlled ultra-short laser pulse fabrication showed up to $\sim 10^2$ times stronger SHG as compared with flat film of gold [9]. The light field enhancement by nano-bumps at the fundamental wavelength was defining the enhancement of SHG. Recently, we showed that the phase control of light reflected and incident on a nanoparticle can enhance surface enhanced Raman scattering (SERS) [10,11]. This mechanism can provide an additional control for the phase sensitive SHG based on the π phase

change upon reflection when light travels through the low-to-high refractive index boundary and the 0 phase change for traversing the high-to-low interface. This mechanism based on Fresnel coefficients is explored in this study together with a propagation phase control by thickness of glass layer.
It was shown recently that optically induced magnetization of gold nanoparticles due to the inverse Faraday effect can be harnessed for non-reciprocal ultra-fast optical rotation [12]. Also, nanoparticles of Ag formed by annealing of the implanted Ag^+ into a Pr:CaF_2 laser crystal host broadens and enhances spectral emission of Pr^{3+} required for a shorter laser pulse generation [13]. The use of nanoparticles and nanostructures in optical control of light enhancement, propagation direction, reflection and NLO effects continues to evolve and widen.
Here, we demonstrate that phase control of light incident and reflected from the layered silica-Si structure allows controlled SHG enhancement. We fabricate and characterise metasurfaces made of plasmonic nanoparticles with a controlled-thickness silica spacer layer on top of a Si substrate. Numerical modeling by finite difference time domain (FDTD) was carried out to reveal characteristics of light field enhancement.

2. Experimental

2.1. Fabrication of metasurfaces

Samples of plasmonic metasurfaces were prepared by standard electron beam lithography (EBL) and lift-off (Fig. 1). A 30-nm-thick gold film was sputtered on a triangular lattice pattern in ZEP520 resist. A thin film of 3 nm of Cr was deposited first for better adhesion of gold. Si(100) wafers were used as a substrate with $w = 200$ and 300 nm thermally-oxidised SiO_2.

2.2. Characterisation of metasurfaces

Extinction - total losses due to absorption and scattering - was measured using a fiber-coupled tungsten-halogen lamp (SLS201L/M, Thorlabs) for the white light source. For the femtosecond laser radiation we used a mode-locked Ti:sapphire oscillator (Tsunami, Spectra-Physics). The oscillation wavelength was tunable between 730 and 920 nm, and the pulse width and repetition rate were ∼100 fs and 75 MHz, respectively. Second harmonic generation (SHG) was measured under wavelength tunable fs-laser irradiation of metasurfaces at normal incidence. Linear polarisation of the incident light at $\lambda = 800$ nm wavelength was set either with $\lambda/2$ or $\lambda/4$-plate. The former was used for rotating the polarisation direction of the linearly-polarised lights. The latter was used for converting the linearly-polarised light into the circularly-polarised lights. Polarisation of second harmonic was interrogated with a Glan-Taylor polariser for the linearly-polarised excitation. The combination of the second $\lambda/4$-plate and the Glan-Taylor polarised was used for analyzing the polarisation state of the SHG waves converted from the circularly-polarised excitation [14].

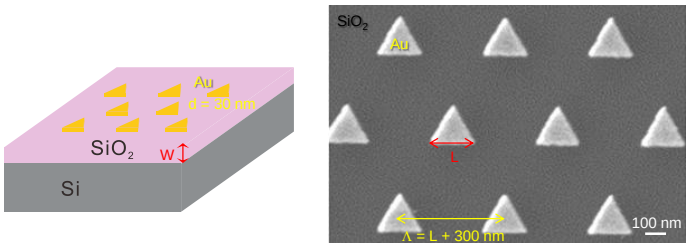

Figure 1. Schematic of the sample (left) and an SEM image of the triangle Au nanoparticles (right). The spacer of SiO_2 with width $w = 200, 300$ nm was deposited on the Si substrate to control the E-field enhancement at the plasmonic Au triangular nanoparticles. The pattern was triangular with period $\Lambda = L + s$ where separation between nanoparticles was $s = 300$ nm and the side-length of the triangle was $L = (120 - 220)$ nm changed in steps of 20 nm. Thickness of Au nanoparticles made by EBL and lift-off was $d = 30$ nm.

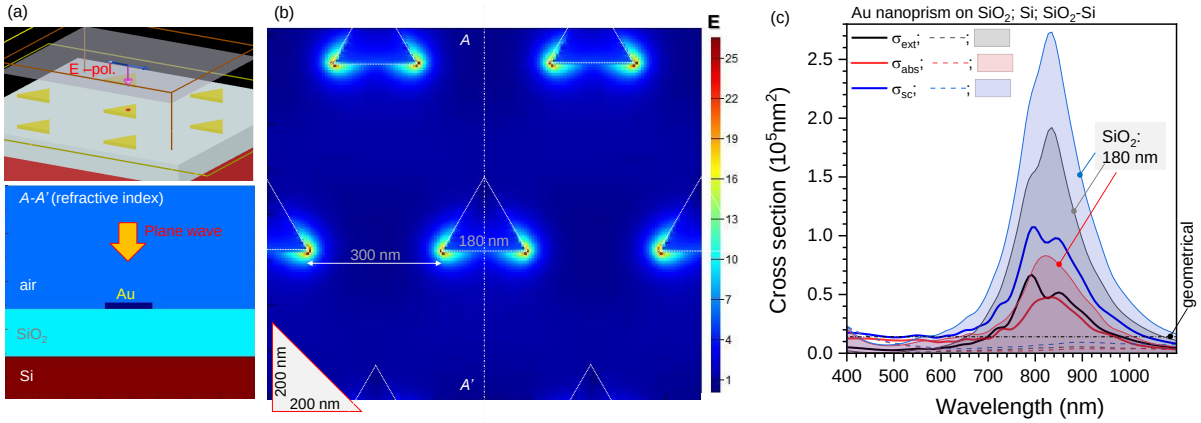

Figure 2. (a) 3D FDTD setting for calculations under linearly polarised (along x-axis) E-field; plane wave illumination. Refractive index cross section (*A*-*A'*). (b) E-field enhancement cross section at the middle-plane of 30-nm-thick Au nano-particles (15 nm above SiO_2). The incident field $|E| = 1$. The maximum field cross section shown is at $\lambda = 825$ nm as in the experiment, see text for discussion. (c) Absorption, scattering and extinction cross sections $\sigma_{ext} = \sigma_{abs} + \sigma_{sc}$ for the $L = 180$ nm nanoprism on SiO_2 (solid lines; refractive index $n = 1.4$), Si (dashed-lines), and SiO_2($w = 180$ nm)-on-Si; optical properties of Si were taken from the material database of Lumerical. The FDTD calculations were carried out using total-field scattered-field (TFSF) light source. Geometrical cross-section corresponds to the footprint area of the nanoprism $S_{Au} = \frac{\sqrt{3}}{4}L^2 \approx 0.1403 \times 10^5$ nm^2.

The SHG signals were detected by liquid nitrogen-cooled CCD camera after being spectrally resolved by multichannel spectrograph (SpectraPro SP-500, Princeton Instruments).

2.3. Numerical modeling

Numerical simulations of light field enhancement were carried out by finite difference time domain (FDTD) method using Lumerical FDTD Solutions. Permittivity of Si, SiO_2, and Au were taken from the database included within the software. Periodic boundary conditions were used for the triangular lattice pattern under auto-optimised mesh size (Fig. 2(a,b)).

Cross sections of absorption σ_{abs}, scattering σ_{sc} and extinction (i.e., the total losses $\sigma_{ext} = \sigma_{abs} + \sigma_{sc}$) were calculated using total-field scattered-field light source (Fig. 2(c)). Nanoprisms with side length of $L = 180$ nm made on SiO_2 or SiO_2-on-Si showed strong scattering around 800 nm wavelength which was used in this study for SHG from such metasurfaces. At this nanoprism size, the scattering is stronger than absorbance which is also important for efficient SHG. Only a SiO_2 spacer thickness of $w = 180$ nm is shown in Fig. 2(c) to illustrate the effect of markedly increased scattering. Nanoprisms on Si had red-shifted resonance and is outside the scope of this study. It is noteworthy, that light E-field enhancement is even stronger at the Au-Si interface as compared with Au-SiO_2 and can be useful for sensor applications in the IR spectral range. These numerical estimates of light absorption and scattering by single nanoprisms was encouragement to embark on fabrication of arrays with different sized nanoprisms on reflective Si substrates with different SiO_2 spacer thicknesses.

3. Results and Discussion

The second-order NLO responses of the metal nanoparticles are expressed by the surface integral of the local non-linear polarisations created on the metal surfaces [15]. The second-order NLO susceptibilities $\chi^{(2)}$ of the metal surfaces are predominantly determined by the surface effects [16–18]. The electric-dipole type selection rule is applied for expressing the non-linear wave conversions on the metal nanoparticles [19]. The geometries of the triangular nanoprisms are classified into *D3h* point group with three non-zero non-linear tensor components $\chi^{(2)}_{yxx}$, $\chi^{(2)}_{yyy}$, and $\chi^{(2)}_{xxy}$ [20], where the

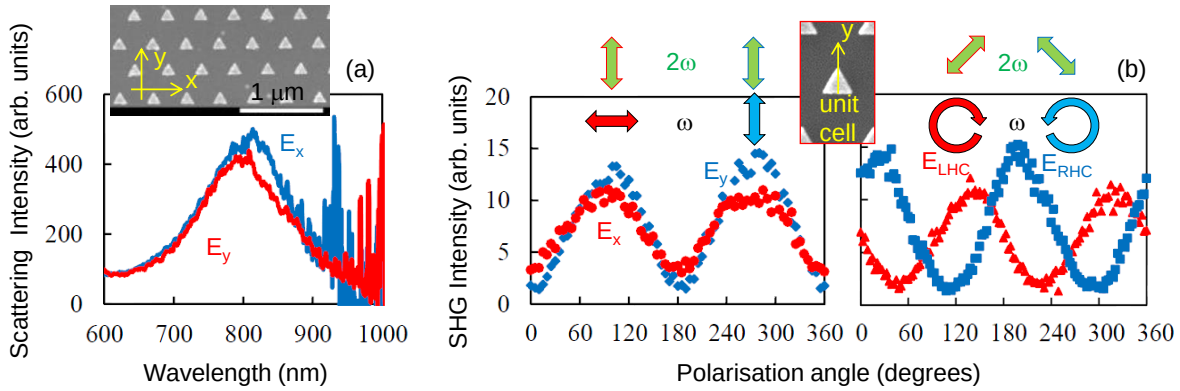

Figure 3. (a) Scattering spectrum of Au nanoprisms on glass for two polarisations in back-scattering geometry. The sizes of the nanoprism were: $L = 150$ nm base of the equilateral triangle, 30 nm thickness, corner-to-corner separation was 250 nm. The prisms arranged two-dimensionally in a trigonal lattice (see SEM image in inset). (b) Polarisation-resolved SHG (2ω) at 800 nm (ω) excitation for different linear and the circular (left- and right-hand) polarisations of excitation in back-scattering/reflection geometry. SHG was y-polarised for different angles of orientation of the incident linearly polarised light (ω). SHG was linearly polarised at $\pm 45^\circ$ from y-axis for the LHC and RHC excitation (ω).

x and y-directions are defined as the base and height directions of the triangular nanoprisms. The field distributions calculated by FDTD distributions were symmetric in the y-axis for both of the pump polarisation geometries and asymmetric in the x-axis. Thus, the SHG emissions along the y-axis was related to breaking symmetry in the x-directions of the electric field, hence, the non-linear tensor components $\chi^{(2)}_{yxx}$ and $\chi^{(2)}_{yyy}$ were responsible for the second-order non-linearities. Next, we tested experimentally the angular dependence of scattering at different excitation wavelengths and polarisation dependence at the maximum of the SHG at 800 nm for nanoprisms on glass samples.

3.1. Au triangular nanoprisms on glass

Figure 3 shows the scattering spectrum from the Au nanoprisms. The scattering spectra were probed by light with polarisations either parallel or perpendicular to the baselines of nanoprisms (x- and y-pol. respectively). The spectral shape of the scattering signal was independent on the polarisation direction of the probe light and peaked at 800 nm. The linear optical properties of the nanoprisms were isotropic. Independent of the polarisation of the excitation, the Au nanorods emitted the SHG at polarisation perpendicular to the baseline of the triangular nanoprism (Fig. 3(b)). The SHG spectroscopy was performed for the nanoprisms with right- and left-handed circular (RHC, LHC) polarised excitation.

The SHG intensities transmitted continuously through the $\lambda/4$-plate and the polariser was the highest at +45° for the LHC excitation and -45° for the RHC (Fig. 3(b)). The form of the nonlinear susceptibility tensor for the *D3h* symmetry demands that the circularly-polarised fundamental light waves are converted into the circularly-polarised SHG waves. The rotation direction of the SHG waves had to be opposite to that of the fundamental. The polarisation state observed by $\lambda/4$-plate and the Glan-Taylor prism is consistent with the expectation imposed by the tensor form for the structures with the *D3h* symmetry [14].

Next, we investigate how SHG can be controlled by increasing light field enhancement at the excitation wavelength.

3.2. Au triangular nanoprisms on Si with SiO_2 spacer

Triangular nanoprisms with different side length from $L = 120$ to 140 nm were fabricated on a strongly reflective Si substrate with two different SiO_2 spacer thicknesses of $w = 200$ nm and 300 nm (Fig. 1).

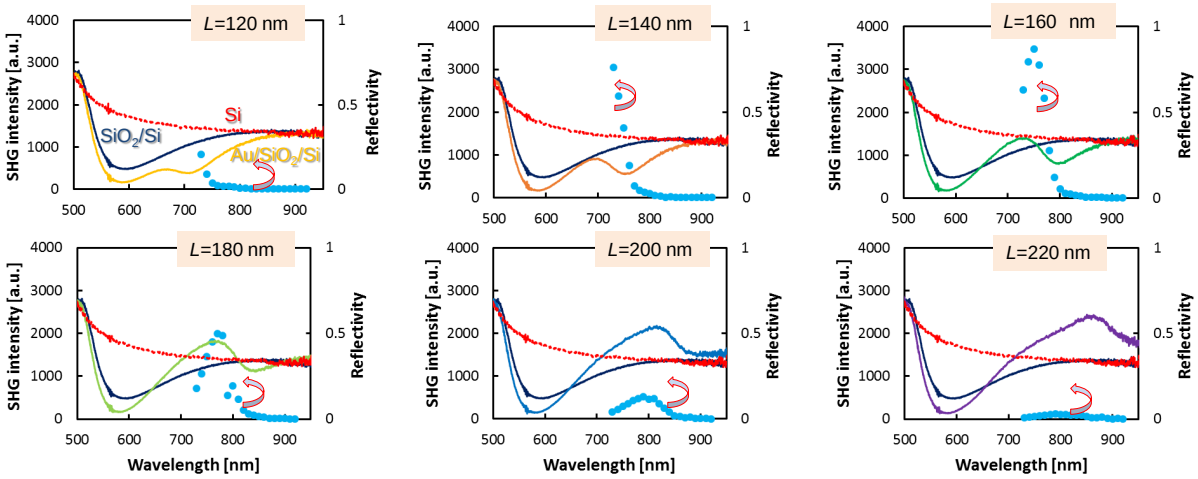

Figure 4. Plots showing experimentally measured SHG excitation spectra from metasurfaces (cyan dots, left-axis) of Au triangular nanoparticles on a SiO_2/Si substrate with triangle side-lengths, $L = 120$ nm to 220 nm. Reflectivity spectra $R(\lambda)$ (right-axis) are shown for bare Si, Si with SiO_2, and the metasurface for each plot. The SiO_2 spacer width was the same $w = 300$ nm (see Fig. A1 for $w = 200$ nm). Polarisation of the incident field was horizontal E_x.

Figures 4 (also, see Fig. A1) summarise reflectivity and SHG results from metasurfaces with different side length L of nanoprisms. The largest spectral sensitivity of SHG vs size of nanoprism L was observed for the thicker $w = 300$ nm spacer (Fig. 4). For thinner $w = 200$ nm, the SHG from $L = 120$ and 140 nm metasurfaces was measurable but at the level of tens-of-counts (Fig. A1) and the strongest SHG was observed for $L = 220$ nm. It is instructive to compare spectral SHG response with reflectivity spectrum. An increase of SHG was observed when the SiO_2 spacer conferred anti-reflective properties to the surface (R smaller as compared with bare Si). The reflectivity of a metasurface with Au nanoprisms is defined by the geometry: period and size of nanoparticles. At peak reflectivity of the fundamental wavelength, the strongest SHG was observed. FDTD simulations confirmed this observation (Fig. 2(b) shows the maximum SHG at $\lambda = 825$ nm). For $w = 200$ nm, SHG was enhanced for larger nanoprisms $L \geq 180$ nm (Fig. A1). Larger triangles formed a larger unit cell of the triangular lattice, hence, the increase of SHG is affected as the ratio of metal area per unit cell, i.e., $S_{Au}/S_{cell} \equiv \frac{L^2}{2\Lambda^2}$, where $\Lambda = L + 300$ nm for the data shown in Figs. 4, A1.

On the resonance at maximum reflectivity, SHG was enhanced more than 3×10^3 times as compared with the non-resonant case (Fig. 4). Also, the maximum of SHG was observed at shorter wavelengths. Obviously the effect of the spacer as a phase retarder for the light reflected from Si on a path to the nanoprism and positively interfering with incident and reflected light from the top of the SiO_2 layer is an important factor. Although the Au nanoprisms were made on Si substrates without SiO_2 spacer, the plasmonic responses were not observed in the present spectral window due to a high ~ 3.7 refractive index of Si causing the localized surface plasmon resonance condition satisfied at much longer wavelengths.

The maximum of SHG had well defined optimal conditions which corresponded to $L = 160$ nm and $w = 300$ nm. FDTD calculations confirmed the strongest light enhancement occurring at the tips of nanoprisms observed at the experimentally determined maximum of SHG enhancement. Figure 5 shows the light field enhancement close to the peak wavelength of SHG for $L = 180$ nm. The enhancement of the E-field more than 50 times was observed and was located at the silica-Au interface. It is noteworthy that the absolute values of enhancement obtained by FDTD should not be considered due to ideal geometrical structures and interfaces being different due to fabrication tolerances [21,22]. The side-view FDTD cross section (Fig. 5) reveals that some of incident light is scattered at larger angles from the direction of propagation at the edges/corners of the nanoprisms. This facilitates light trapping in silica (between air and Si) which contributes to light enhancement at

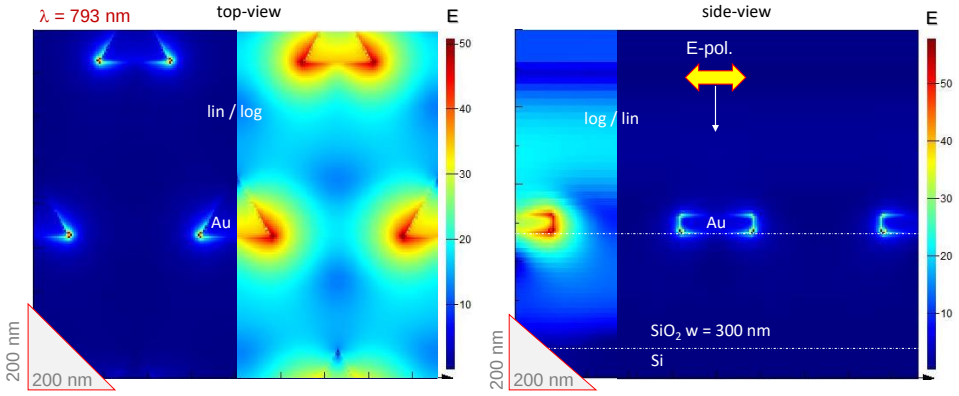

Figure 5. FDTD at the maximum E-field enhancement for $L = 180$ nm and $w = 300$ nm (see Fig. 4). The top-view monitor is at the air-silica interface and the side-view monitor crosses the side of triangle and vertexes with the highest field enhancement. The E-field scale bars are linear; polarisation of incident field was horizontal E_x.

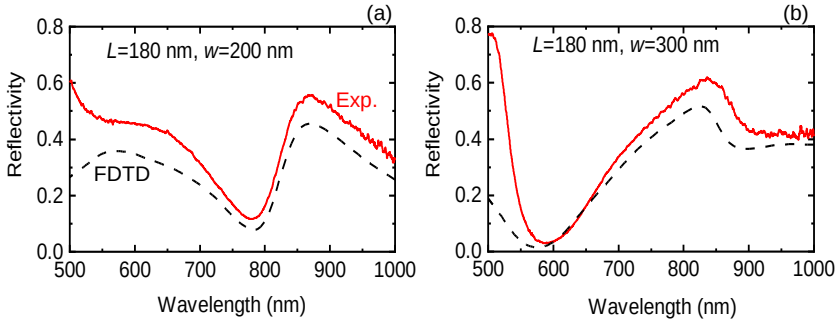

Figure 6. Experimental (Exp; red) and calculated (FDTD; dashed) reflectivity spectra of Au nanoprisms with $L = 180$ nm side length. The thicknesses of the SiO_2 spacer were (a) $w = 200$ nm and (b) 300 nm.

neighbouring nanoprisms.

The maximum of SHG is red-shifted for larger nano-triangles. This tendency was confirmed by FDTD simulations (Fig. A2). The maximum of E-field enhancement was observed at 924 nm wavelength ($L = 220$ nm) as compared with 825 nm for the $L = 180$ nm. The pattern of E-field enhancement was qualitative same, the vertexes of equal-side triangles which are aligned to the polarisation of incident plane wave are enhanced. The peak enhancement up to $E = 30$ times was observed at the maximum (incident field $E = 1$). Side-view of E-field distribution shows even stronger localization at the SiO_2-air-Au point (note, the lateral cross sections are shown at 15 nm above the interface at the middle thickness of Au nanoparticle). These locations of largest E-field locatization at the interface are locations for SHG. From the side-view image it is also clear that some light was deposited into the SiO_2 spacer which also facilitates field enhancement at the neighbouring nanoparticles.

Figure 6 shows direct comparison between experimentally measured reflectivity R together with FDTD numerical results for the two tested spacer thicknesses. Maximum of R was a good predictor for the most efficient SHG and a good match between theoretical estimates and experimentally measured R values was observed at the peak of SHG. It could be envisaged that by using different 2D and 3D nanofabrication techniques including direct laser writing [23–26] it should be possible to inscribe non-centrosymmetric patterns into the interface or fill by NLO polymers rendering such meta-surfaces/materials as efficient SHG materials [27]. The use of reflective plasmonic non-centrosymmetric patterns are very promising for nanoscale engineering of SHG [28,29]. The presented triangular symmetric *D3h* pattern of nanoprisms can be used to enhance SHG from 2D materials of the same symmetry, e.g., WSe_2, which showed SHG from monolayer flakes [30]. Also,

photo and thermally induced material re-organisation can be used for breaking usually random orientation and symmetry of polymers to make them active for SHG [31]. Use of anisotropic bio-polymers such as silk [32] and nanocellulose [33] and their polymer composites is another way to make host materials for the anisotropic light-matter interaction required for SGH.

4. Conclusions and Outlook

It is demonstrated that SHG from non-centro-symmetric triangular nanoprisms can be enhanced using a SiO_2 spacer between the nanoprisms and Si substrate. Experimental results proved that the Au nanoprisms are well suited for harnessing second-order non-linearities at normal incidence conditions at the nanoscale. The polarisation dependence of SHG showed that at the linearly polarised fundamental wave the SHG was always y-polarised, independent of the polarisation of the excitation light. For the circularly polarised excitation, the SHG was also circularly polarised with the handedness opposite to the excitation light as expected from the *D3h* symmetry.

By optimising the thickness of the SiO_2 spacer it is possible to maximise SHG generation by several orders of magnitude. It is expected that this method will allow achievement of high yield SHG from films of non-linear optical (NLO) materials placed on metasurfaces: $I(2\omega) \propto |\chi^{(2)}_{meta} + \chi^{(2)}_{NLO} \times d_{NLO}|^2 I^2(\omega)$, where $I(\omega)$ is light intensity at the fundamental wavelength ($\lambda = 2\pi c/\omega$) which is locally enhanced at the nanoscale on the nanoprisms, d_{NLO} is the thickness of the non-linear optical material which is expected to be thin for best harvesting of the local field enhancement. Metasurfaces of nanoparticles are expected to be able to withstand higher light intensities without degradation and has to be investigated next. As polymers enters the second century of their development [34], a combination of new polymers with augmented functionalities and metasurfaces will bring new science and applications.

Author Contributions: Conceptualisation, A.S; methodology, A.S.; validation, A.S.,S.J.; formal analysis, A.S.; investigation (experimental), K.M., M.S., H.Y.; investigation (numerical) M.S., S. L., J.H. S.H.N.; resources, A.S.; data curation, A.S., S.H.N., Y.N.; writing—original draft preparation, A.S., S.J.; writing—review and editing, all the authors; visualisation, K.M., H.Y.; supervision, A.S.; project administration, A.S.; funding acquisition, A.S.

Funding: This work was supported by Nippon Sheet Glass Co., Ltd. grant, JST CREST Grant Number JPMJCR19I3, Japan and the ARC Discovery DP190103284 and Linkage LP190100505 grants.

Acknowledgments: Support of operational costs of the Nanotechnology facility (2016-2019) by Swinburne Univ. Technol. is acknowledged. Visits of Shizuoka University students to present their research at the student research biannual workshop "Fast-Small", Swinburne 2012-19 were supported by the SSSV (Exhibition of Laboratory Exchange Program) program of Shizuoka Univ. MS is grateful for the support from Shizuoka Univ. for a research stay at Swinburne Univ. in 2019-20.

Conflicts of Interest: The authors declare no conflict of interest.

Appendix A Reflection and SHG spectra for $w = 200$ nm SiO_2 on Si

Experimental spectra of reflectivity and SHG are overlayed for the metasurfaces with the side length of the nanoprism ranging from $L = 120$ nm to 220 nm for the SiO_2 spaced $w = 200$ nm in Fig. A1 (see main text for $w = 300$ nm in Fig. 4).

Figure A2 presents summary a of FDTD modeling of the light field enhancement for the $w = 200$ nm SiO_2 spacer at several wavelengths. The inset "ray-box" shows schematics of interference taking place on the front surface as addition of the SiO_2-reflected and Si-reflected rays. Each of them experience π phase shift due to reflectance from the medium with a higher refractive index. The Si-reflected ray has additional propagation phase traversing the SiO_2 spacer twice. When the spacer is close to the $\lambda/4$ condition, a constructive E-field addition takes place on the air-SiO_2 surface (where Au nanoprisms are positioned). The actual field values depend on the Fresnel coefficients, which are, in turn, incidence angle dependent. This interference and phase matching is the physical reason for the increased SHG efficiency with the optimised thickness of SiO_2 spacer around $w = 300$ m [10]. Such description is strictly valid for the optical far-field representation of reflection and the actual near-field conditions where diffraction from the Au nanoprisms is taking place is accounted for in the

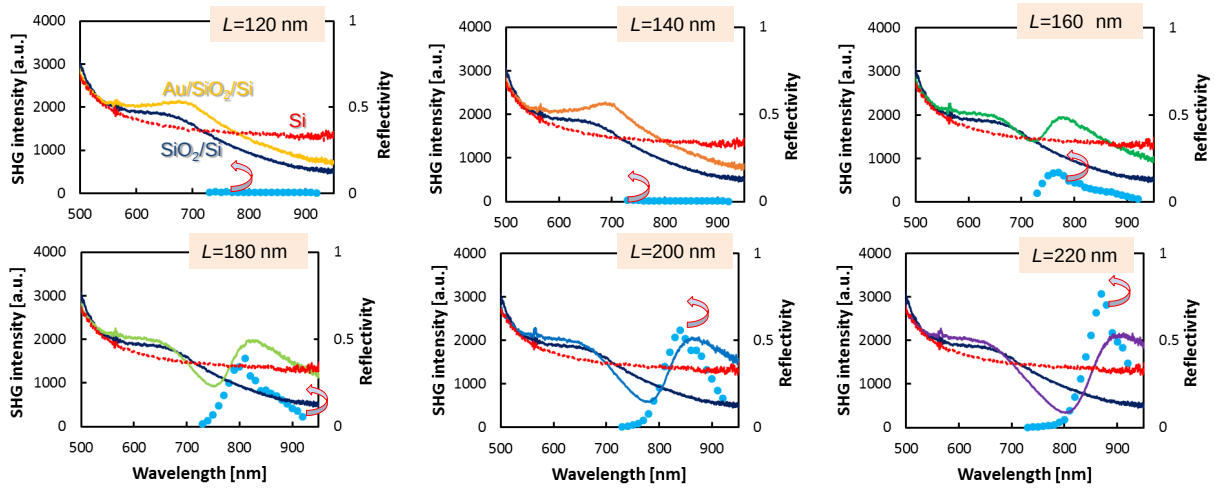

Figure A1. Plots showing experimentally measured SHG excitation spectra from metasurfaces (cyan dots, left-axis) of Au triangular nanoparticles on a SiO_2/Si substrate with triangle side-lengths, $L =$ 120 nm to 220 nm. Reflectivity spectra $R(\lambda)$ (right-axis) are shown for bare Si, Si with SiO_2, and the metasurface for each plot. The SiO_2 spacer width was the same $w = 200$ nm. Polarisation of the incident field was horizontal E_x.

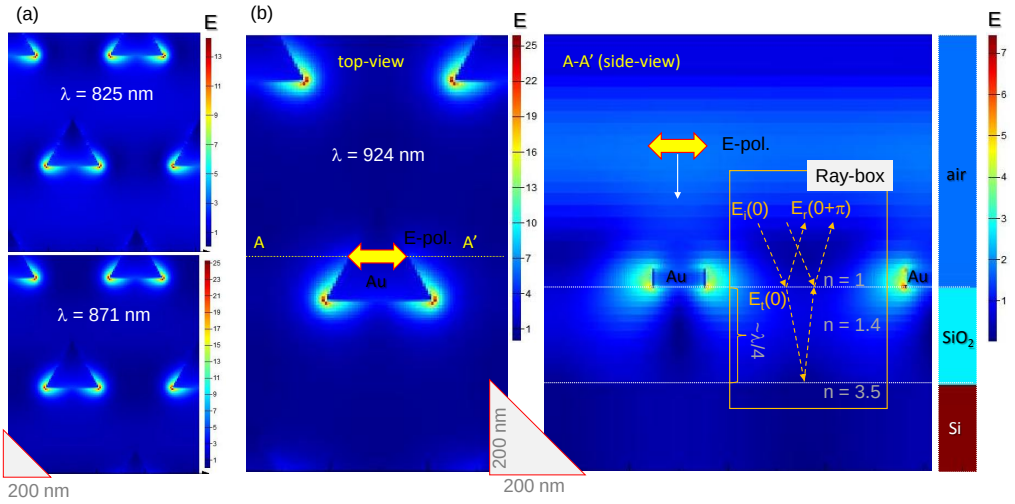

Figure A2. FDTD simulations for the $L = 220$ nm $w = 200$ nm case. (a) E-field enhancement at $\lambda = 825$ nm (see Fig. 2(b) for comparison) and 871 nm which are close-to-maximum. (b) Top- and side views of E-field enhancement for a linearly polarised plane wave. Refractive index cross-section is shown on right-side to distinguish the lateral cross-sections. Note, the cross-section A-A' is made though the center of triangle and not at the largest intensity vertexes. Incident light has E_x polarisation. Inset "ray-box" shows schematically the phase change upon reflection from interfaces for the incident, transmitted and reflected E-fields $E_{i,t,r}$ in ray optics presentation [10]. In addition to the Fresnel coefficient defined phase changes, a propagation phase is adding up and amounts to π for traversing a $\lambda/4$ thickness twice upon back-reflection from Si.

FDTD simulations. More systematic studies are required for the dependence of SHG from the spacer thickness w. Here, only two thicknesses $w = 200$ nm and 300 nm were tested.

References

1. Sun, Q.C.; Ding, Y.C.; Sagar, D.M.; Nagpal, P. Photon upconversion towards applications in energy conversion and bioimaging. *Progr. Surface Sci.* **2017**, *92*, 281–316.

2. Wen, S.; Zhou, J.; Schuck, P.J.; Suh, Y.D.; Schmidt, T.W.; Jin, D. Future and challenges for hybrid upconversion nanosystems. *Nature Photonics* **2019**, *13*, 828–838.
3. Zhou, J.; Chizhik, A.I.; Chu, S.; Jin, D. Single-particle spectroscopy for functional nanomaterials. *Nature* **2020**, *579*, 41–50.
4. Aouani, H.; Rahmani, M.; Navarro-Cía, M.; Maier, S.A. Third-harmonic-upconversion enhancement from a single semiconductor nanoparticle coupled to a plasmonic antenna. *Nature Nanotech.* **2014**, *9*, 290–294.
5. Kauranen, M.; Zayats, A.V. Nonlinear plasmonics. *Nano Lett.* **2012**, *6*, 737–748.
6. Butet, J.; Brevet, P.R.; Martin, O.J.F. Optical second harmonic generation in plasmonic nanostructures: from fundamental principles to advanced applications. *ACSNano* **2015**, *9*, 10545–10562.
7. Krasnok, A.; Tymchenko, M.; Alù, A. Nonlinear metasurfaces: a paradigm shift in nonlinear optics. *Materials Today* **2014**, *21*, 8–21.
8. Guixin, L.; Shuang, Z.; Thomas, Z. Nonlinear photonic metasurfaces. *Nat. Rev. Mater.* **2017**, *2*, 17010.
9. Cherepakhin, A.B.; Pavlov, D.V.; Shishkin, I.I.; Voroshilov, P.M.; Juodkazis, S.; Makarov, S.V.; Kuchmizhak, A.A. Laser-printed hollow nanostructures for nonlinear plasmonics. *Appl. Phys. Lett.* **2020**, *117*, 041108.
10. Zheng, Y.; Rosa, L.; Thai, T.; Ng, S.H.; Juodkazis, S.; Bach, U. Phase controlled SERS enhancement. *Sci. Reports* **2019**, *9*, 744.
11. Jayawardhana, S.; Rosa, L.; Juodkazis, S.; Stoddart, P.R. Additional Enhancement of Electric Field in Surface-Enhanced Raman Scattering due to Fresnel Mechanism. *Sci. Rep.* **2013**, *3*, 2335.
12. Cheng, O.H.C.; Son, D.H.; Sheldon, M. Light-induced magnetism in plasmonic gold nanoparticles. *Nature Photonics* **2020**, *14*, 365–368.
13. Nie, W.; Jiang, S.; Li, R.; Ren, F.; Clayton, A.; Juodkazis, S.; Chen, F. Plasmon-induced photoluminescence and Raman enhancement in Pr:CaF_2 crystal by embedded silver nanoparticles. *Appl. Surf. Sci.* **2020**, *530*, 147018.
14. Konishi, K.; Higuchi, T.; Li, J.; Larsson, J.; Ishii, S.; Kuwata-Gonokami, M. Polarization-Controlled Circular Second-Harmonic Generation from Metal Hole Arrays with Threefold Rotational Symmetry. *Phys. Rev. Sci. Lett.* **2014**, *112*, 135502.
15. O'Brien, K.; Suchowski, H.; Rho, J.; Salandrino, A.; Kante, B.; Yin, X.; Zhang, X. Predicting nonlinear properties of metamaterials from the linear response. *Nature Mater.* **2015**, *14*, 379–383.
16. Wang, F.X.; Rodriguez, F.J.; Albers, W.M.; Ahorinta, R.; Sipe, J.E.; Kauranen, M. Surface and bulk contribution to the second-order nonlinear optical response of a gold film. *Phys. Rev. B* **2009**, *80*, 233402.
17. Sipe, J.E.; So, V.C.Y.; Fukui, M.; Stegemann, G.I. Analysis of second-harfnonic generation at metal surfaces. *Phys. Rev B* **1980**, *21*, 4389–4402.
18. Maytorena, J.A.; Mochan, W.L.; Mendoza, B.S. Hydrodynamic model for second-harmonic generation at conductor surfaces with continuous profiles. *Phys. Rev B* **1995**, *51*, 2556–2562.
19. Canfield, B.K.; Husu, H.; Laukkanen, J.; Bai, B.; Kuittinen, M.; Turunen, J.; Kauranen, M. Local Field Asymmetry Drives Second-Harmonic Generation in Noncentrosymmetric Nanodimers. *Nano Lett.* **2007**, *7*, 1251–1255.
20. Boyd, R.W., Nonlinear Optics; Academic press: Cambridge, Massachusetts, 2008; chapter 1. The nonlinear optical susceptibility, p. 1.
21. Nishijima, Y.; Balcytis, A.; Naganuma, S.; Seniutinas, G.; Juodkazis, S. Tailoring metal and insulator contributions in plasmonic perfect absorber metasurfaces. *ACS Appl. Nano Mater.* **2018**, *1*, 3557–3564.
22. To, N.; Nishijima, Y.; Juodkazis, S. Detailed Experiment-Theory Comparison of Mid-Infrared Metasurface Perfect Absorbers. *Micromachines* **2020**, *11*, 409.
23. Yamasaki, K.; Juodkazis, S.; Matsuo, S.; Misawa, H. Three-dimensional microchannels in polymers: one step fabrication. *Appl. Phys. A* **2003**, *77*, 371–373.
24. Buividas, R.; Rekštytė, S.; Malinauskas, M.; Juodkazis, S. Nano-groove and 3D fabrication by controlled avalanche using femtosecond laser pulses. *Opt. Mat. Express* **2013**, *3*, 1674–1686.
25. Seet, K.K.; Mizeikis, V.; Juodkazis, S.; Misawa, H. Three-Dimensional Horizontal Circular Spirals Photonic Crystals with stop gaps below 1 μm. *Appl. Phys. Lett.* **2006**, *88*, 221101.
26. Li, Z.Z.; Wang, L.; Fan, H.; Yu, Y.H.; Chen, Q.D.; Juodkazis, S.; Sun, H.B. O-FIB: far-field-induced near-field breakdown for direct nanowriting in an atmospheric environment. *Light: Sci. Appl.* **2020**, *9*, 052003.

27. Sugita, A.; Ito, K.; Sato, Y.; Suzuki, R.; Sato, K.; Narumi, T.; Mase, N.; Takano, Y.; Matsushita, T.; Tasaka, S.; Kawata, Y. The role of chemisorption for push-pull chromophores on SiO_2 surfaces in non-electrically poling host-guest NLO polymers. *J Photochem Photobiol A: Chem.* **2017**, *340*, 35–45.
28. Yogo, H.; Matsui, T.; Nihashi, S.; Hirabayashi, T.; Inami, W.; Ono, A.; Kawata, Y.; Sugita, A. Polarized second-harmonic-generation spectroscopy for Au nanorods arrayed on SiO_2 substrates at localized surface plasmon resonances. *Jpn J Appl Phys* **2017**, *56*, 122002.
29. Sugita, A.; Kaname, S.; Mochizuki, K.; Kikuchi, K.; Ono, A.; Inami, W.; Kawata, Y. Second harmonic conversions of surface-plasmon-polariton-enhanced optical fields in nonlinear optics polymer/Ag/glass structures. *Phys Rev B* **2020**, *101*, 045303.
30. Rosa, H.G.; Ho, Y.W.; Verzhbitskiy, I.; Rodrigues, M.; Taniguchi, T.; Watanabe, K.; Eda, G.; Pereira, V.M.; Gomes, J. Characterization of the second- and third-harmonic optical susceptibilities of atomically thin tungsten diselenide. *Sci. Reports* **2018**, *8*, 10035.
31. Makihara, K.; Kaneta, D.; Iwamura, T.; Sugita, A.; Leproux, P.; Couderc, V.; Kano, H. Photo-induced meta-stable polar conformations in polystyrene microspheres revealed by time-resolved SHG microscopy. *Appl Phys Express* **2020**, *13*, 052003.
32. Ryu, M.; Honda, R.; Reich, A.; Cernescu, A.; Li, J.L.; Hu, J.; Juodkazis, S.; Morikawa, J. Near-Field IR Orientational Spectroscopy of Silk. *Appl. Sci.* **2019**, *9*, 3991.
33. Fujisawa, H.; Ryu, M.; Lundgaard, S.; Linklater, D.P.; Ivanova, E.P.; Nishijima, Y.; Juodkazis, S.; Morikawa, J. Direct Measurement of Temperature Diffusivity of Nanocellulose-Doped Biodegradable Composite Films. *Micromachines* **2020**, *11*, 738.
34. Abd-El-Aziz, A.S.; Antonietti, M.; Barner-Kowollik, C.; Binder, W.H.; Böker, A.; Boyer, C.; Buchmeiser, M.R.; Cheng, S.Z.D.; D'Agosto, F.; Floudas, G.; Frey, H.; Galli, G.; Genzer, J.; Hartmann, L.; Hoogenboom, R.; Ishizone, T.; Kaplan, D.L.; Leclerc, M.; Lendlein, A.; Liu, B.; Long, T.E.; Ludwigs, S.; Lutz, J.F.; Matyjaszewski, K.; Meier, M.; Müllen, K.; Müllner, M.; Rieger, B.; Russell, T.P.; Savin, D.A.; Schlüter, A.D.; Schubert, U.S.; Seiffert, S.; Severing, K.; Soares, J.; Staffilani, M.; Sumerlin, B.; Sun, Y.; Tang, B.; Tang, C.; Théato, P.; Tirelli, N.; Tsui, O.; Unterlass, M.; Vana, P.; Voit, B.; Vyazovkin, S.; Weder, C.; Wiesner, U.; Wong, W.Y.; Wu, C.; Yagci, Y.; Yuan, J.; Zhang, G. The Next 100 Years of Polymer Science. *Macromol. Chem. Phys.* **2020**, *2020*, 2000216.